26 Radiative-Decay Engineering: Surface Plasmon-Coupled Emission

In the preceding chapter we described the use of metallic particles to modify emission. This was accomplished by interaction of the excited dipoles of the fluorophore with oscillating electrons in a nearby metallic surface. We used the term "metal" to describe such surfaces. We described how a fluorophore near a metal can have a different radiative-decay rate. This is an unusual effect because this rate does not change substantially when a fluorophore is in different environments.

In this chapter we describe another phenomenon that occurs when a fluorophore is near a metal. Under certain circumstances a fluorophore can couple with a continuous metallic surface to create groups of oscillating electrons called surface plasmons. If the metal film is thin and on an appropriate substrate the plasmons radiate their energy into the substrate. We call this phenomenon surface plasmon-coupled emission (SPCE).[1] There are numerous potential applications for this phenomenon that efficiently collects the emission and transforms it into directional radiation.

26.1. PHENOMENON OF SPCE

Prior to describing the theory for SPCE it is informative to describe this phenomenon (Figure 26.1). Suppose an excited fluorophore is positioned above a thin silver film, where the metal film is continuous and about 50 nm thick. Such films are visually opaque. Remarkably, the emission from the fluorophore is not reflected but is efficiently transferred through the film. The spatial distribution of fluorescence is isotropic or nearly isotropic. However, the emission seen through the film occurs only at a unique angle θ_F measured from the normal. Since the sample is symmetric about the normal z-axis the emission occurs as a cone around the axis. This cone is not due to selective transmission of emission through the film. A large fraction of the total emission appears in the cone. About half of the emission appears in the cone and about half is free-space emission away from the film. The emission in the cone has the same emission spectrum as the fluorophore.

The light from the excited fluorophore appearing in the cone is called surface plasmon-coupled emission (SPCE).[1] This name reflects our current understanding of the phenomenon. We believe the excited fluorophore creates surface plasmons in the metal. These plasmons do not appear to be the result of RET to the surface because the distances over which SPCE occurs are too large for RET. SPCE occurs over distances up to 200 nm or 2000 Å, which are much larger than Förster distances near 50 Å. The plasmons radiate into the substrate at an angle determined by the optical properties of the metal and substrate. Since the wavelength distribution of SPCE is the same as the fluorophore emission it is tempting to assume it originates from the fluorophore. However, the emission is 100% p-polarized, even if the fluorophores are randomly oriented and excited with unpolarized light. See Chapter 2 for a definition of p-polarization. This polarization indicates the surface plasmons are radiating and not the fluorophores.

26.2. SURFACE-PLASMON RESONANCE

The phenomenon of SPCE appears to be closely related to surface-plasmon resonance (SPR). SPR is now widely used in the biosciences and provides a generic approach to measurement of biomolecule interactions on surfaces.[2–6] A schematic description of SPR is shown in Figure 26.2. The measurement is based on the interaction of light with thin metal films on a glass substrate. The film is typically made of gold 40–50 nm thick. The surface contains a capture bio-

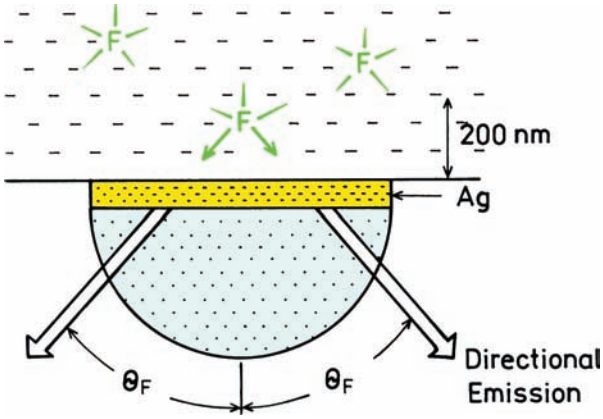

Figure 26.1. Surface plasmon-coupled emission. F is a fluorophore.

molecule that has affinity for the analyte of interest. The capture biomolecule is typically covalently bound to the gold surface. This sample is optically coupled to a hemispherical or hemicylindrical prism by an index-matching fluid. Light impinges on the gold film through the prism, which is called the Kretschmann configuration. The instrument measures the reflectivity of the gold film at various angles of incidence (θ), with the same angle used for observation (θ).

The usefulness of SPR is due to the dependence of the reflectivity of the gold film on the refractive index of the solution immediately above the gold film. The angle-dependent reflectivity of the gold surface is dependent on the refractive index of the solution because there is an evanescent field extending from the gold surface into the solution. Binding of macromolecules above the gold film

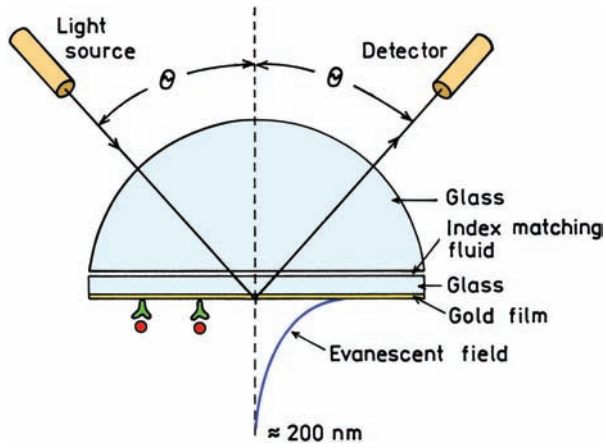

Figure 26.2. Typical configuration for surface-plasmon resonance analysis. The incident beam is p-polarized.

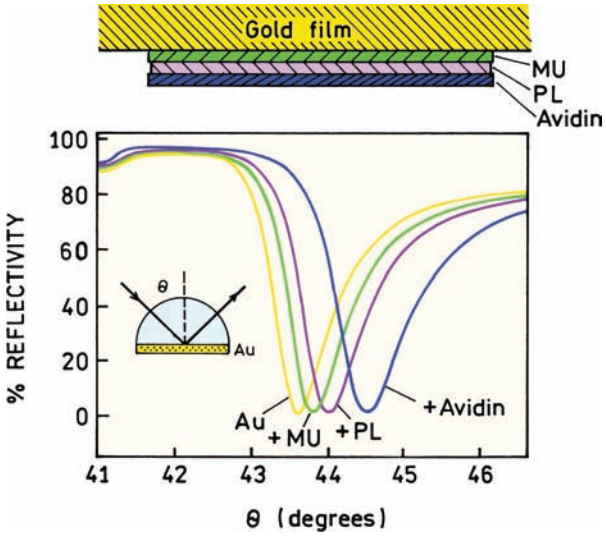

Figure 26.3. SPR reflectivity curves for a 47-nm gold film on BK-7 glass. Illumination was at 633 nm. The gold film was progressively coated with 11-mercaptoundecanoic acid (MU), followed by biotinylated poly-lysine (PL), and then avidin. Adapted from [7–9].

causes small changes in the refractive index, which result in changes in reflectivity. Figure 26.3 shows typical SPR data: a plot of reflectivity versus the angle of incidence for a 47-nm gold film.[7–9] The reflectivity minimum occurs at the SPR angle. The SPR angles change as the gold surface is coated with 11-mercaptoundecanoic acid (MU), then biotinylated polylysine (PL), and finally avidin. The changes in SPR angle are due to changes in the refractive index near the gold surface due to the adsorbed layers.

The decrease in reflectivity at the SPR angle (θ_{SP}) is due to absorption of the incident light at this particular angle of incidence. At this angle the incident light is absorbed and excites electron oscillations on the metal surface. The reflectivity is sensitive to the refractive index because of the evanescent field that penetrates approximately 200 nm into the solution (Figure 26.2). The evanescent field appears whenever there is resonance between the incident beam and the gold surface. An evanescent field is not present when there is no plasmon resonance, that is, when the reflectivity is high.

The existence of an evanescent field is reminiscent of total internal reflectance (TIR), which occurs between a glass–water interface when the angle of incidence from the glass slide exceeds the critical angle.[10] There can be confusion about the relationship between the critical angle in TIR (θ_C) and the SPR angle (θ_{SP}). The physical origins of θ_C and θ_{SP} are similar, in that both are dependent on wavevector

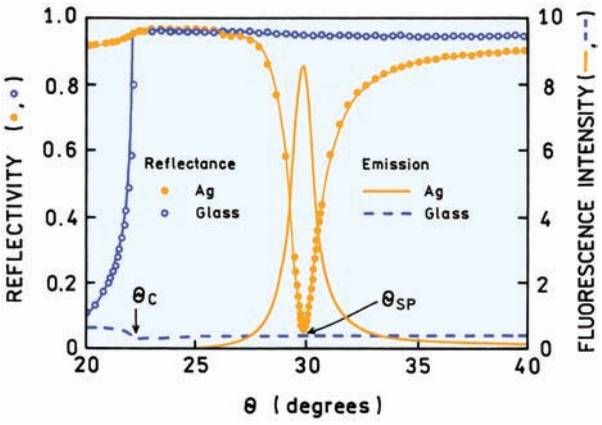

Figure 26.4. Reflectivity curves for a bare glass and silver-coated glass, both spin coated with a fluorophore in polyvinyl alcohol. The prism is LaSFN9 glass, 633 nm. Also shown is the fluorescence from the labeled PVA film on the glass and silver surfaces. Adapted from [11].

matching at the sample–glass or metal interface. However, these angles are different and not directly related. This difference between θ_C and θ_{SP} is illustrated in Figure 26.4, which compares glass and silver–coated glass surfaces.[11–12] The silver-coated surface shows high reflectivity at all angles except around the plasmon angle near 30°. The reflectivity of a glass surface is quite different. The reflectivity is low below the critical angle θ_C, increases sharply to nearly 100% at θ_C, and remains high for all angles above θ_C. For the glass surface and angles above θ_C there exists an evanescent field from the totally internally reflected light. For the silver-coated glass there is no evanescent field in the aqueous phase unless the angle of incidence is near the SPR angle. The reflectivity of the silver film is high at angles significantly larger or smaller than θ_{SP}.

The evanescent wave due to SPR is much more intense than that due to TIR.[11–17] The relative strengths of the fields can be measured by the fluorescence from fluorophores near the surface. For the sample shown in Figure 26.4 fluorophores were localized within the evanescent field by coating with a polyvinyl alcohol (PVA) film that contained a fluorophore. The dependence of the emission on the incident angle indicates the relative intensity of the evanescent wave felt by the fluorophores. For the glass surface the emission intensity is low for $\theta < \theta_C$. This low value is essentially the same as seen in a typical fluorescence measurement where the fluorophore is excited in a glass or quartz cuvette. As the incident angle exceeds θ_C the intensity drops about twofold because the incident light undergoes TIR rather than passing into the sample. Above the critical angle the remaining intensity represents the amount of excitation due to the TIR evanescent wave. This result indicates that the field strength for TIR is roughly the same for the incident light and the evanescent wave.

Different results are seen for the labeled film on the silver surface. The emission intensity is near zero for angles above and below θ_C because of the high reflectivity of the metal film. In contrast to uncoated glass, the light does not penetrate the sample even though $\theta < \theta_C$. There is a dramatic increase in the emission intensity of the film near the plasmon angle: about 15-fold. This effect is due to a 10- to 40-fold increase in the intensity of the evanescent field above silver as compared to above glass with TIR.[18–21] This increase in field strength above a metal film is one origin of the increased sensitivity possible with plasmon-coupled emission.

An important characteristic of the SPR angles is that they are strongly dependent on wavelength. Figure 26.5 shows the reflectivity curves of a gold film for several wavelengths.[22] The surface plasmon angle decreases as the wavelength decreases. The dependence on wavelength can be understood in terms of the optical constants of the metals, which depend upon wavelength (frequency) and the dielectric constant of the adjacent prism. This dependence of θ_{SP} on wavelength is the origin of intrinsic spectral resolution when observing surface plasmon-coupled emission.

26.2.1. Theory for Surface-Plasmon Resonance

An understanding of SPR is useful for understanding surface plasmon-coupled emission. The theory to describe the reflectivity of metal-coated surfaces is complex. It can be difficult to understand the underlying physical interactions that are responsible for angle-dependent absorption. We will not describe the detailed equations needed to calculate the reflectivity.

The phenomenon of SPR can be understood by considering the propagation constant of the incident electromagnetic wave across the surface of the metal, along the *x*-axis. An electromagnetic wave propagating in space can be described by

$$\bar{E}(\bar{r},t) = \bar{E}_0 \exp(i\omega t - i\bar{k} \cdot \bar{r}) \qquad (26.1)$$

where the bars indicate vector quantities, $\bar{r}$ is a unit vector in the direction of propagation, ω is the frequency in radians/s, $i = -1^{1/2}$, and · indicates the dot product. The term k

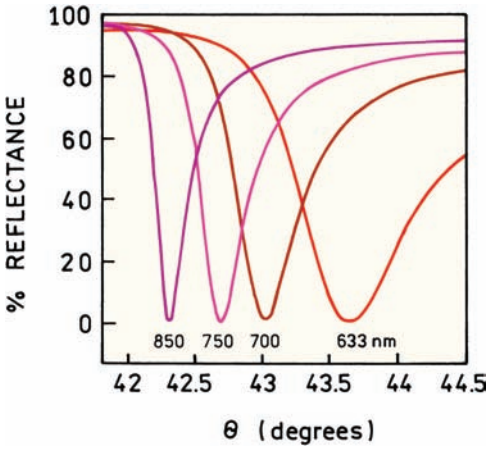

Figure 26.5. Calculated wavelength-dependent reflectivity for a 47-nm-thick gold film. From [22].

is the propagation constant, which is sometimes called the wavevector. This value is given by

$$k = \frac{2\pi}{\lambda} = \frac{n\omega}{c} = nk_0 \tag{26.2}$$

where $\lambda = \lambda_0/n$ is the wavelength, λ_0 is the wavelength in a vacuum, n is the refractive index of the medium, and k_0 is the propagation constant of the wave in a vacuum. It is understood that the physical values are given by the real part of eq. 26.1. Hence the electric field is described by

$$\overline{E}(\bar{r},t) = \overline{E}_0 \exp(\cos\omega t - \overline{k} \cdot \bar{r}) \tag{26.3}$$

For SPR we need to consider the electric field along the x-axis at the metal–water interface. This component is given by

$$E(x,t) = E_{0x} \exp(\cos\omega t - k_x x) \tag{26.4}$$

To satisfy Maxwell's equations the electric fields have to be continuous across the interface, which requires k_x to be equal in both media.

The phenomenon of SPR can be understood by considering the propagation constant of the electromagnetic wave in the metal along the x-axis. In the metal film the field is described by eqs. 26.3 and 26.4 with $k_x = k_r + ik_{im}$ being the complex wavevector along the x-axis. For a metal the propagation constant for the surface plasmon is given by

$$k_{SP} = \frac{\omega}{c}\left(\frac{\varepsilon_m\varepsilon_s}{\varepsilon_m + \varepsilon_s}\right)^{1/2} = k_0\left(\frac{\varepsilon_m\varepsilon_s}{\varepsilon_m + \varepsilon_s}\right)^{1/2} \tag{26.5}$$

where ε_m and ε_s are the dielectric constant of the metal (m) and sample (s), respectively. ε_s refers to the effective dielectric constant in the region of the evanescent field (Figure 26.2). Because the real part of ε_m is larger than the imaginary part the propagation constant can be approximated by

$$k_{SP} = k_0\left(\frac{\varepsilon_r\varepsilon_s}{\varepsilon_r + \varepsilon_s}\right)^{1/2} \tag{26.6}$$

The incident light can excite a surface plasmon when its x-axis component equals the propagation constant for the surface plasmon (Figure 26.6). The propagation constant for the incident light in the prism (p) is given by

$$k_p = k_0 n_p \tag{26.7}$$

and the component along the x-axis is equal to

$$k_x = k_0 n_p \sin\theta_p \tag{26.8}$$

where θ_p is the incidence angle in the prism. Hence the conditions for SPR absorption is satisfied when

$$k_{SP} = k_x = k_0 n_p \sin\theta_{sp} \tag{26.9}$$

where θ_{sp} is the angle of incidence in the metal for surface-plasmon resonance to occur. These considerations show

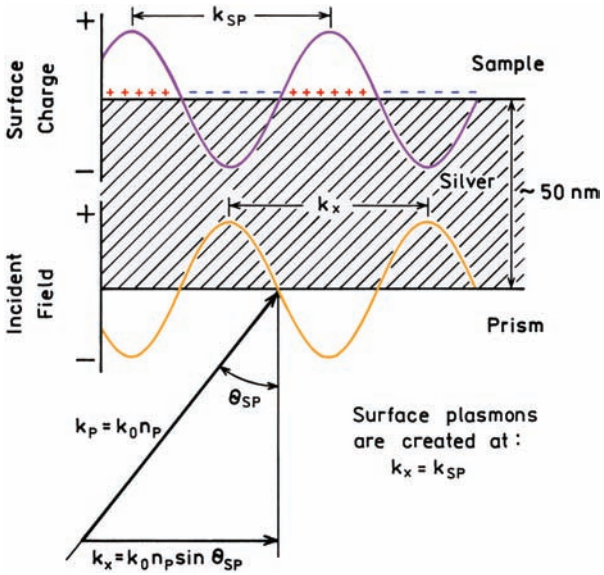

Figure 26.6. Schematic showing propagation constants in a prism and a thin film.

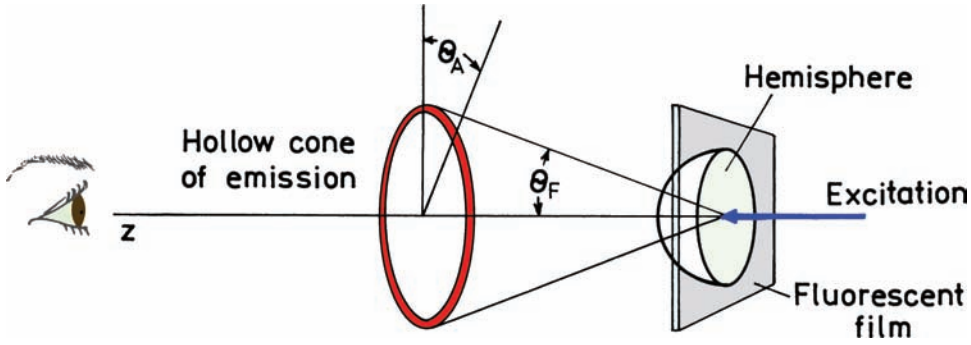

Figure 26.7. Surface plasmon-coupled cone of emission for fluorophores near a metallic film.

that the surface-plasmon resonance occurs whenever the *x*-axis component of the incident field equals that obtained from eq. 26.5.

A mental picture of SPR can be found by considering the wavelength of the incident light in the prism and the projection of this distance onto the interface (Figure 26.6). SPR occurs when this projected distance matches the wavelength of the surface plasmon. This visualization of SPR explains the increase in θ_p needed for resonance at shorter wavelengths.

26.3. EXPECTED PROPERTIES OF SPCE

The previous explanation of SPR allows us to make several predictions for the properties of SPCE. The fluorophores are randomly distributed and the sample can be excited with unpolarized light. There is no preferential direction around the *z*-axis. Hence the SPCE is expected to appear as a cone around the *z*-axis (Figure 26.7). Figure 26.5 shows that SPR occurred at different angles of incidence for different wavelengths. The analogy with SPR suggests different emission wavelengths will appear at different angles (Figure 26.8). Hence the SPCE is expected to appear as a circular rainbow with the range of colors determined by the emission wavelength range of the fluorophore. In SPR only p-polarized incident light is absorbed. This suggests the SPCE will also be p-polarized around the *z*-axis. The polarization is expected to point radially away from the *z*-axis at all positions about the *z*-axis.

26.4. EXPERIMENTAL DEMONSTRATION OF SPCE

It was important to have an experimental demonstration of SPCE. The sample was sulforhodamine 101 (S101) in a 15-nm-thick PVA film.[23] The film was on a 50-nm-thick layer of silver. Figure 26.9 shows the angular distribution of the emission which is distributed sharply at ±47° from the normal. Integration of the angle-dependent emission, and the free-space emission away from the hemispherical prism, indicated that about half of the emission is contained in the directional component exiting through the prism.

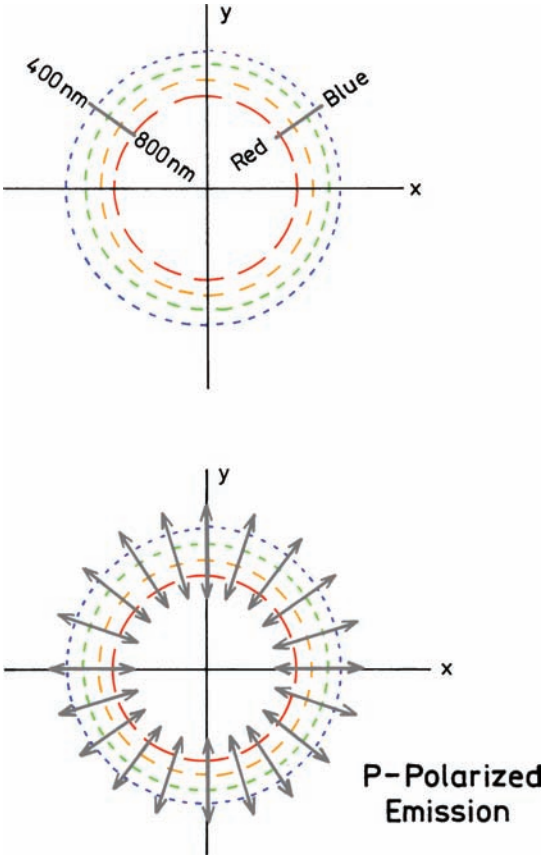

Figure 26.8. Color distribution and polarization expected for SPCE.

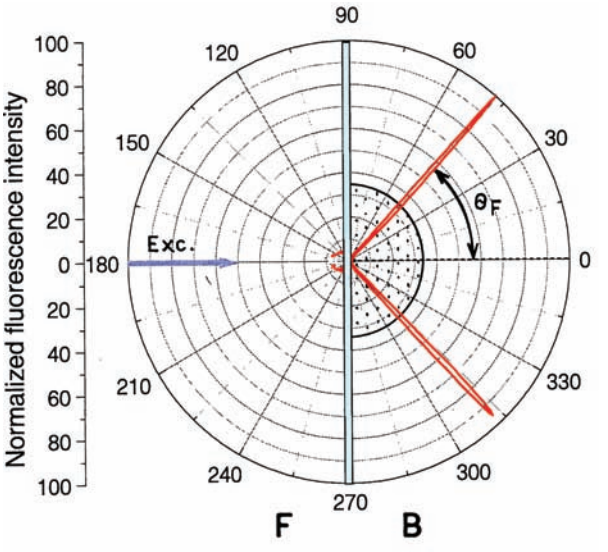

Figure 26.9. Angular distribution of the SPCE from sulforhodamine 101 (S101) in a 15-nm PVA film using the reverse Kretschmann configuration. From [23].

We also tested if the wavelength dependence seen for SPR (Figure 26.5) occurred for SPCE. A mixture of three fluorophores was used to obtain a wider range of wavelengths. The SPCE was found to be dispersed at different angles according to the wavelength (Figure 26.10) in the same direction as the SPR absorption. This result shows that a simple metal film can be used to efficiently collect the emission from nearby fluorophores, convert the emission to directional emission, and disperse the emission according to wavelength.

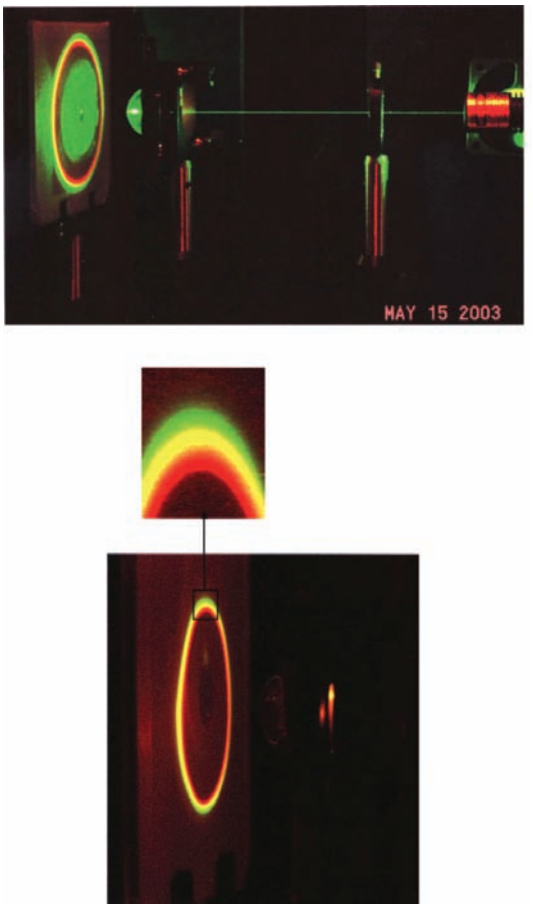

Figure 26.10. Photograph of SPCE from the mixture of fluorophores using RK excitation and a hemispherical prism, 532 nm excitation. From [23].

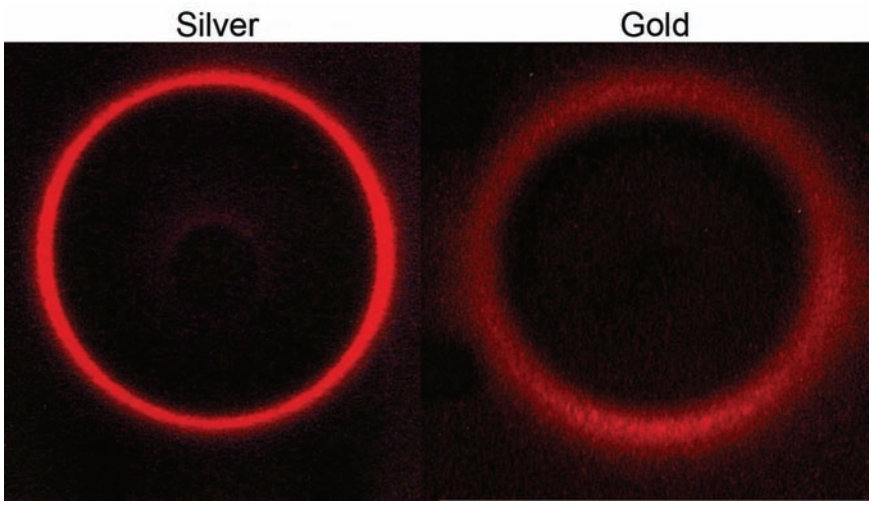

Figure 26.11. Cone of emission for S101 in PVA on silver and gold films.

In the application of SPCE it would be an advantage to use gold rather than silver surfaces. Gold does not tarnish and the chemistry for coating the surface with organic molecules is more highly developed for gold than silver. However, in contrast to silver, gold is known to quench fluorescence.[24–26] Fortunately, gold can be used for SPCE (Figure 26.11).[27] The angular distribution is slightly wider on gold than on silver, which is a result of its different optical properties. The reason gold does not quench in SPCE is because of the longer distances for SPCE as compared to Förster transfer, which is probably the mechanism by which gold quenches fluorescence.

SPCE is due mostly to fluorophores within about 200 nm of the surface. This suggests the possibility of selective observation of fluorophores localized near the metal surface. We tested this possibility by adding a "background" fluorophore more distant from the metal. This was accomplished by making the coated silver film part of a 1-mm-thick demountable cuvette. The cuvette was filled with a solution of rhodamine 6G in ethanol. PVA is weakly soluble in ethanol and the dyes remained separate for the course of the experiments. The free-space emission was observed at 149° and the SPCE at 77°. The concentrations were chosen so that the free-space emission was dominated by the R6G background (Figure 26.12). Even with this large background signal the SPCE was dominated by S101, which is closer to the metal film. The PVA thickness was only 30 nm, so that some R6G was present within the distance for SPCE, accounting for the remaining intensity of R6G at 550 nm. More effective background suppression can be expected with a thicker PVA or sample film to keep this impurity more distant from the metal film.

26.5. APPLICATIONS OF SPCE

Since SPCE occurs for fluorophores near surfaces it will most likely be used with surface-based assays. One expected advantage of SPCE is the suppression of unwanted background because fluorophores distant from the metal surface will not create surface plasmons and SPCE. For this assay the surface-bound antibody was rabbit IgG (Figure 26.13). This surface was incubated with rhodamine-labeled anti-rabbit IgG and Alexa 647-labeled anti-mouse IgG. The later antibody does not bind to the surface and serves as the unwanted background.

Figure 26.14 shows the emission spectra of the free-space and surface-plasmon coupled emission. The free-space emission is dominated by the Alexa 647 background. In contrast, the SPCE is due mostly to the surface-bound antibody. This result shows that SPCE can be used to selectively observe fluorophores near the metal surface and to effectively decrease the amount of background emission. SPCE provides a potentially simple approach for improved performance in a wide variety of surface-bound arrays.

Intrinsic biochemical fluorophores such as tryptophan emit at ultraviolet wavelengths. It is possible to imagine many biochemical applications of SPCE occurring at shorter wavelengths. SPCE of UV-emitting fluorophores has

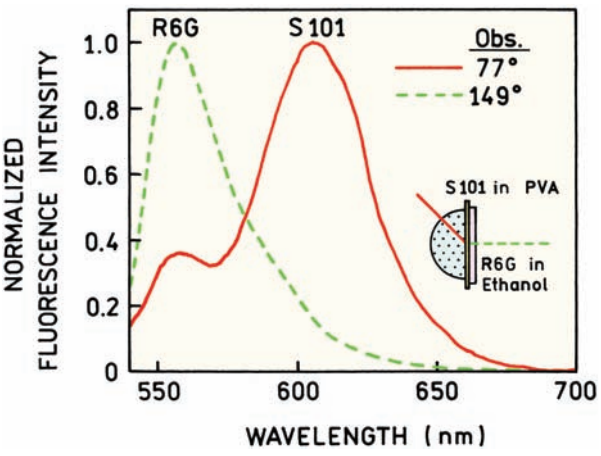

Figure 26.12. Emission spectra of S101 in PVA with simulated background emission from rhodamine 6G (R6G). The concentration of S101 in the PVA film was about 10 mM and the concentration of R6G in ethanol about 5 μM. From [23].

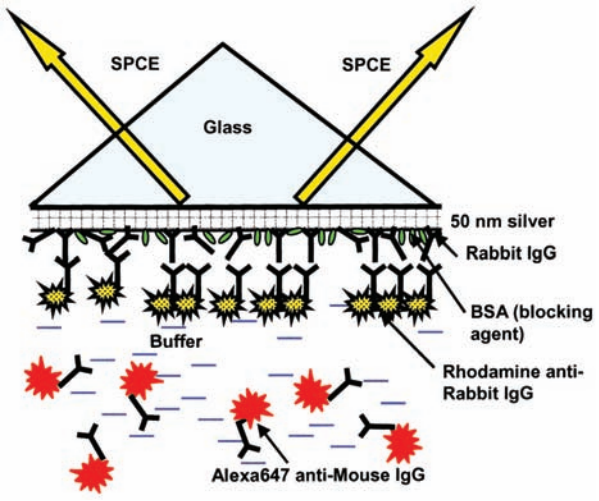

Figure 26.13. SPCE immunoassay. Anti-rabbit antibodies (labeled with Rhodamine Red-X) bind to rabbit IgG immobilized on the silver surface. Non-binding anti-mouse antibodies labeled with Alexa Fluor 647 remain in solution. From [28].

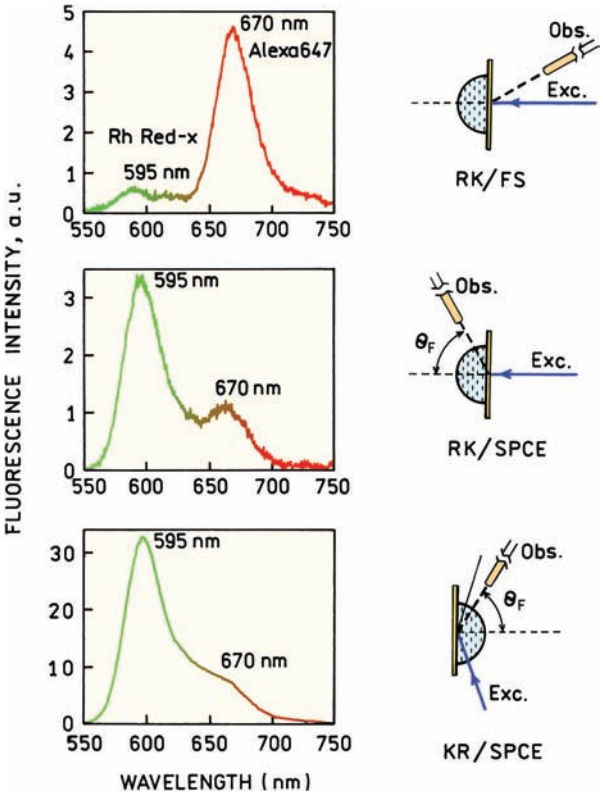

Figure 26.14. Emission spectra of the rhodamine red-X labeled anti-rabbit antibodies bound to rabbit IgG immobilized on a 50-nm silver mirror surface in the presence of a fluorescent background (anti-mouse antibodies labeled with Alexa Fluor 647). Top, free-space emission. Bottom, SPCE. From [28].

been observed with aluminum films [29–31] Figure 26.15 shows the angle-dependent emission of 2-aminopurine in PVA on a 20-nm-thick aluminum film. Once again SPCE occurs over a narrow angular distribution, but the distribution is wider than that found for silver (Figure 26.9). This wider angular distribution is a result of the optical properties of aluminum and appears to result in a greater angular dispersion of different wavelengths (Figure 26.16). The apparent emission spectra of 2-AP are strongly dependent on the observation angle.

26.6. FUTURE DEVELOPMENTS IN SPCE

SPCE offers numerous opportunities for new types of assays and sample configurations. A guiding concept may be the radiating plasmon (RP) model.[32] This model suggests that the optical and geometric properties of the sample can be chosen so that plasmons can radiate effectively and in the desired direction. An example of this approach is for a thin silver grating.

Excited fluorophores near such a grating display plasmon-coupled emission through the grating, with different wavelengths appearing at different angles. Plasmon-coupled emission through the grating provides opportunities for novel fluorescence-sensing configurations. Figure 26.17 shows an example where a sensing layer is positioned above the thin film grating. Emission from the sensing layer will couple through the grating and could be observed with

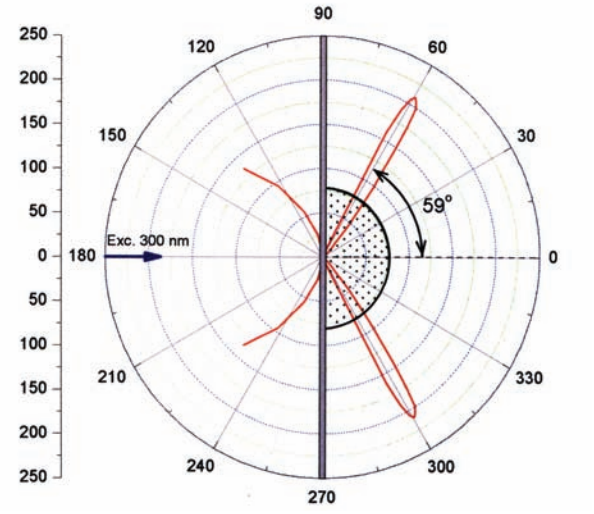

Figure 26.15. Angle-dependent SPCE of 2-aminopurine (2-AP) at 380 nm with reverse Kretschmann excitation. 2-AP is in a PVA film. Revised and reprinted with permission from [39]. Copyright © 2004, American Chemical Society.

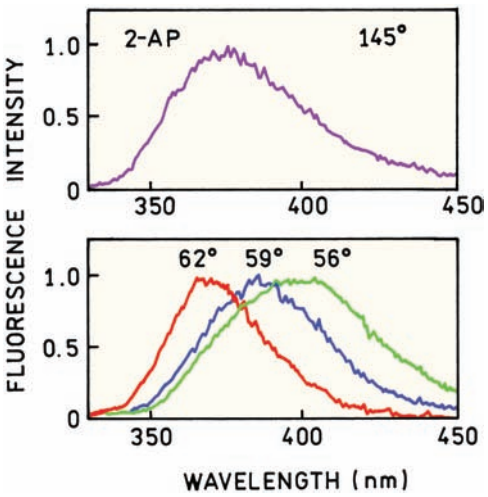

Figure 26.16. Free-space (top) and SPCE (bottom) of 2-AP. The emission spectra were recorded at different observation angles. Revised and reprinted with permission from [30]. Copyright © 2004, American Chemical Society.

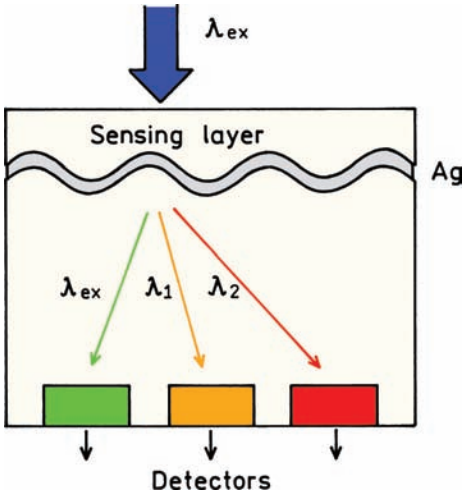

Figure 26.17. Fluorescence-sensing module based on grating-coupled plasmon emission.

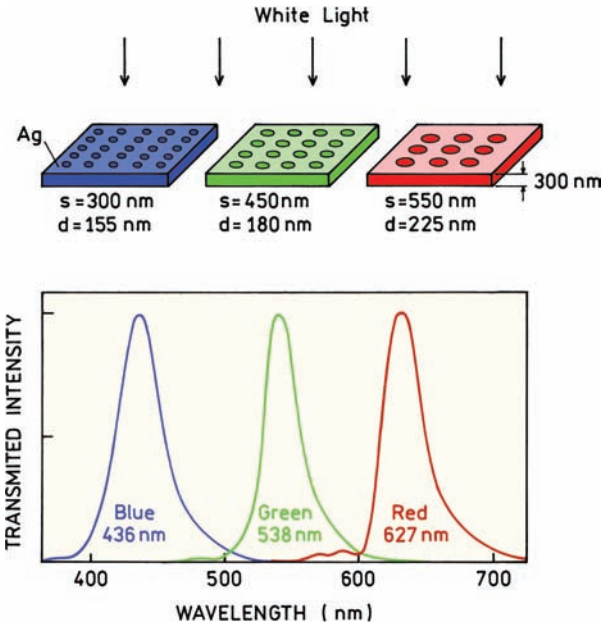

Figure 26.18. Light transmission through perforated but otherwise opaque silver films. s and d refer to the interhole spacing and diameter, respectively. Figure drawn from results in and reprinted with permission from [34]. Copyright © 2004, American Chemical Society.

closely spaced and/or proximity focused detectors. Ratiometric sensing should be possible using the wavelength separation provided by the grating. The application of SPCE will be guided by theory that is becoming more refined.[32–33]

In 1998 a report appeared which showed that thick metal films with a regular array of sub-wavelength-size holes can display extraordinary optical transmission greatly in excess of the transmission expected based on the open area of the holes.[34] This effect is shown schematically in Figure 26.18. The silver film was 300 nm thick, which is opaque in the absence of holes. If the films contained nanoholes there was efficient transmission through the films, much more efficient than would be expected from the size of the holes. The transmitted wavelength depended on the size and spacing of the holes. This observation resulted in theoretical studies to explain this effect.[35–37] It is now thought that the transmission is due to the creation of surface plasmons on one surface, migration of the plasmons through the holes, and subsequent radiation of the plasmons from the distal side of that metal. Such films should be useful in fluorescence devices. The transmitted radiation is strongly dependent on wavelength, so that the films may be used as both an excitation filter and/or for the creation of far-field radiation (Figure 26.19). For example, the hole

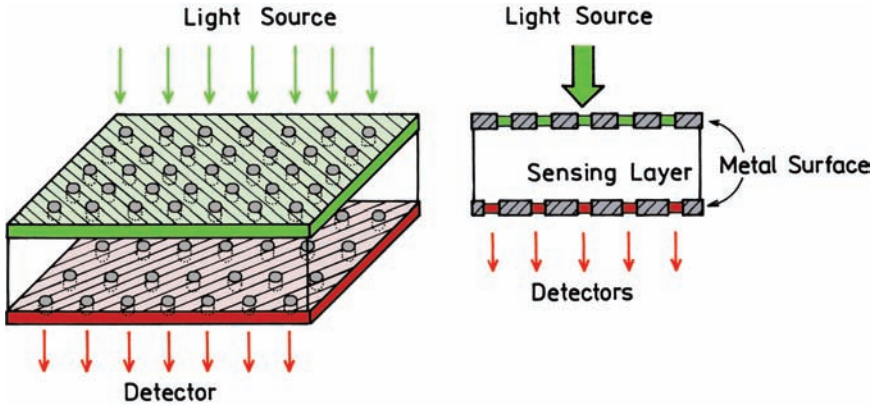

Figure 26.19. Fluorescence-sensing device base on plasmon transport through a metal surface with a regular array of holes.

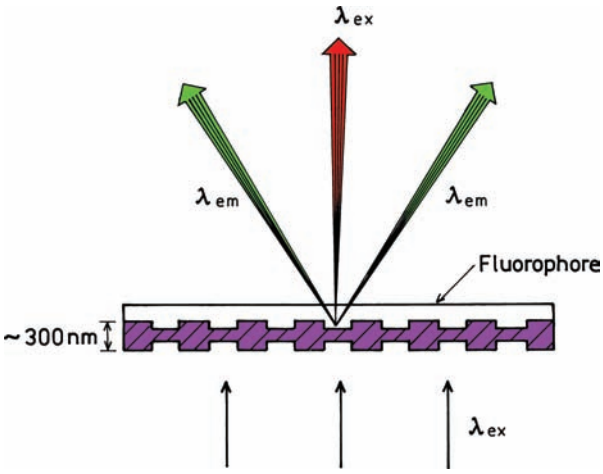

Figure 26.20. Directional and diffracted emission from a fluorophore on a metal film with linear opening. Adapted from [38].

spacing of the top metal layer could be selected to transmit the excitation wavelength, and the spacing in the lower layer selected to transmit the emission wavelength.

Even more elegant configurations are possible by combining plasmon engineering with nanoengineering, which can be used to obtain strongly directional emission. One example is shown in Figure 26.20 for an array of parallel lines etched through the metal.[38–40] This structure serves as a type of monochromator in that light near 600 nm is transmitted most efficiently. Importantly, the transmitted light radiates only at defined directions into the far field on the distal side of the metal and the various wavelengths radiate in different directions. An even more remarkable result is shown in Figure 26.21 for a metal film with open concentric rings. In addition to being wavelength selective, the transmitted light migrates as a narrow beam into the far field.

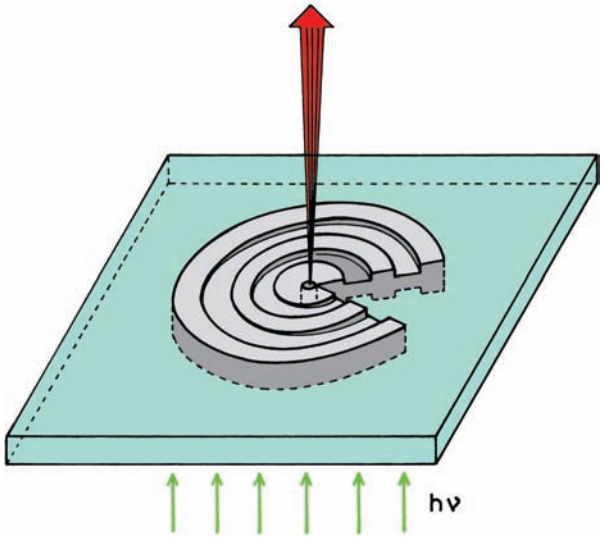

Figure 26.21. Directional emission from a fluorophore on a metal film with open concentric rings. Adapted from [38].

These optical transmission phenomenon can be used with the properties of radiating plasmons to design novel fluorescence devices which serve as both the excitation filter and, more importantly, to focus the emission in the desired direction and pattern. Using the concept that if a plasmon can radiate it will, fluorophores could be placed on either side of the films shown in Figures 26.20 and 26.21. Depending on the geometry of the film and the optical constants of all the materials, fluorophores on or near the metal will transfer to the plasmons, which in turn will radiate according to electromagnetic theory.

In closing, we believe the rational design of metallic structures that couple with fluorophores and efficiently radiate the energy will provide the basis for a new generation of nanooptical sensing devices.

REFERENCES

1. Lakowicz JR. 2004. Radiative decay engineering, 3: surface plasmon-coupled directional emission. *Anal Biochem* **324**:153–169.
2. Salamon Z, Macleod HA, Tollin G. 1997. Surface plasmon resonance spectroscopy as a tool for investigating the biochemical and biophysical properties of membrane protein systems, I: theoretical principles. *Biochim Biophys Acta* **1331**:117–129.
3. Melendez J, Carr R, Bartholomew DU, Kukanskis K, Elkind J, Yee S, Furlong C, Woodbury R. 1996. A commercial solution for surface plasmon sensing. *Sens Actuators B* **35–36**:212-216.
4. Liedberg B, Lundstrom I. 1993. Principles of biosensing with an extended coupling matrix and surface plasmon resonance. *Sens Actuators B* **11**:63–72.
5. Cooper MA. 2002. Optical biosensors in drug discovery. *Nature Rev* **1**:515–528.
6. Wegner GJ, Lee HJ, Corn RM. 2002. Characterization and optimization of peptide arrays for the study of epitope–antibody interactions using surface plasmon resonance imaging. *Anal Chem* **74**:5161–5168.
7. Frutos AG, Corn RM. 1998. SPR of utrathin organic films. *Anal Chem* **70**:449A–455A.
8. Jordan CE, Frey BL, Kornguth S, Corn RM. 1994. Characterization of Poly-L-lysine adsorption onto alkanethiol-modified gold surfaces with polarization-modulation fourier transform infrared spectroscopy and surface plasmon resonance measurements. *Langmuir* **10**:3642–3648.
9. Frey BL, Jordan CE, Kornguth S, Corn RM. 1995. Control of the specific adsorption of proteins onto gold surfaces with poly(l-ysine) monolayers. *Anal Chem* **67**:4452–4457.

10. Axelrod D, Hellen EH, Fulbright RM. 1992. Total internal reflection fluorescence. In *Topics in fluorescence spectroscopy*, Vol 3: *Biochemical applications*, pp. 289–343. Ed JR Lakowicz. Plenum Press, New York.
11. Neumann T, Johansson ML, Kambhampati D, Knoll W. 2002. Surface-plasmon fluorescence spectroscopy. *Adv Funct Mater* **12**: 9–575-586.
12. Liebermann T, Knoll W. 2000. Surface-plasmon field-enhanced fluorescence spectroscopy. *Colloids Surf* **171**:115–130.
13. Ekgasit S, Stengel G, Knoll W. 2004. Concentration of dye-labeled nucleotides incorporated into DNA determined by surface plasmon resonance-surface plasmon fluorescence spectroscopy. *Anal Chem* **76**:4747–4755.
14. Ekgasit S, Thammacharoen C, Yu F, Knoll W. 2004. Evanescent field in surface plasmon resonance and surface plasmon field-enhanced fluorescence spectroscopies. *Anal Chem* **76**:2210–2219.
15. Roy S, Kim J-H, Kellis JT, Poulose AJ, Robertson CR, Gast AP. 2002. Surface plasmon resonance/surface plasmon enhanced fluorescence: an optical technique for the detection of multicomponent macromolecular adsorption at the solid/liquid interface. *Langmuir* **18**:6319–6323.
16. Yokota H, Saito K, Yanagida T. 1998. Single molecule imaging of fluorescently labeled proteins on metal by surface plasmons in aqueous solution. *Phys Rev Lett* **80**(20):4606–4609.
17. Yu F, Persson B, Löfås S, Knoll W. 2004. Attomolar sensitivity in bioassays based on surface plasmon fluorescence spectroscopy. *J Am Chem Soc* **126**:8902–8903.
18. Attridge JW, Daniels PB, Deacon JK, Robinson GA, Davidson GP. 1991. Sensitivity enhancement of optical immunosensors by the use of a surface plasmon resonance fluoroimmunoassay. *Biosens Bioelectron* **6**:201–214.
19. Liebermann T, Knoll W, Sluka P, Herrmann R. 2000. Complement hybridization from solution to surface-attached probe-oligonucleotides observed by surface-plasmon-field-enhanced fluorescence spectroscopy. *Colloids Surf* **169**:337–350.
20. Fukuda N, Mitsuishi M, Aoki A, Miyashita T. 2002. Photocurrent enhancement for polymer Langmuir–Blodgett monolayers containing ruthenium complex by surface plasmon resonance. *J Phys Chem B* **106**:7048–7052.
21. Stengel G, Knoll W. 2005. Surface plasmon field-enhanced fluorescence spectroscopy studies of primer extension reactions. *Nucleic Acids Res* **33**(7):e69.
22. Natan MJ, Lyon LA. 2002. Surface plasmon resonance biosensing with colloidal Au amplification. In *Metal nanoparticles: synthesis, characterization, and applications*, pp. 183–205. Ed DL Feldheim, CA Foss. Marcel Dekker, New York.
23. Gryczynski I, Malicka J, Gryczynski Z, Lakowicz JR. 2004. Radiative decay engineering, 4: experimental studies of surface plasmon-coupled directional emission. *Anal Biochem* **324**:170–182.
24. Thomas KG, Kamat PV. 2003. Chromophore-functionalized gold nanoparticles. *Acc Chem Res* **36**:888–898.
25. Kamat PV. 2002. Photophysical, photochemical, and photocatalytic aspects of metal nanoparticles. *J Phys Chem B* **106**(32):7729–7744.
26. Du H, Disney MD, Miller BL, Krauss TD. 2003. Hybridization-based unquenching of DNA hairpins on Au surfaces: prototypical 'molecular beacon' biosensors. *J Am Chem Soc* **125**:4012–4013.
27. Gryczynski I, Malicka J, Gryczynski Z, Lakowicz JR. 2004. Surface plasmon-coupled emission with gold films. *J Phys Chem* **108**: 12568–12574.
28. Matveeva E, Gryczynski Z, Gryczynski I, Lakowicz JR. 2004. Immunoassays based on directional surface plasmon coupled emission. *J Immunol Methods* **286**:130–140.
29. Malicka J, Gryczynski I, Gryczynski Z, Lakowicz JR. 2004. Surface plasmon-coupled ultraviolet emission of 2,5-diphenyl-1,3,4-oxadiazole. *J Phys Chem B* **108**:19114–19118.
30. Gryczynski I, Malicka J, Gryczynski Z, Nowaczyk K, Lakowicz JR. 2004. Ultraviolet surface plasmon-coupled emission using thin aluminum films. *Anal Chem* **76**:4076–4081.
31. Gryczynski I, Malicka J, Lukomska J, Gryczynski Z, Lakowicz JR. 2004. Surface plasmon-coupled polarized emission of N-acetyl-L-tryptophanamide. *Photochem Photobiol* **80**(3):482–485.
32. Calander N. 2004. Theory and simulation of surface plasmon-coupled directional emission from fluorophores at planar structures. *Anal Chem* **76**:2168–2173.
33. Lakowicz JR. 2004. Radiative decay engineering, 5: metal-enhanced fluorescence and plasmon emission. *Anal Biochem* **337**:171–194.
34. Ebbesen TW, Lezec HJ, Ghaemi HF, Thio T, Wolff PA. 1998. Extraordinary optical transmission through sub-wavelength hole arrays. *Nature* **381**:667–669.
35. Bonod N, Enoch S, Li L, Popov E, Neviere M. 2003. Resonant optical transmission through thin metallic films with and without holes. *Optics Express* **11**(5):482–490.
36. Zayats AV, Salomon L, De Fornel F. 2003. How light gets through periodically nanostructured metal films: a role of surface polaritonic crystals. *J Microsc* **210**(3):344–349.
37. Thio T, Lezec HJ, Ebbesen TW, Pellerin KM, Lewen GD, Nahata A, Linke RA. 2002. Giant optical transmission of sub-wavelength apertures: physics and applications. *Nanotechnology* **13**:429–432.
38. Martin-Moreno L, Garcia-Vidal FJ, Lezec HJ, Degiron A, Ebbesen TW. 2003. Theory of highly directional emission from a single subwavelength aperture surrounded by surface corrugations. *Phys Rev Lett* **90**(16):167401-1–167401-4.
39. Garcia-Vidal FJ, Lezec HJ, Ebbesen TW, Martin-Moreno L. 2003. Multiple paths to enhance optical transmission through a single subwavelength slit. *Phys Rev Lett* **90**(21):213901-1–213901-4.
40. Lezec HJ, Degiron A, Devaux E, Linke RA, Martin-Moreno L, Garcia-Vidal FJ, Ebbesen TW. 2002. Beaming light from a subwavelength aperture. *Science* **297**:820–822.